



Review

Recent Developments of TiO₂-Based Photocatalysis in the Hydrogen Evolution and Photodegradation: A Review

Baglan Bakbolat ^{1,2}, Chingis Daulbayev ^{1,2,3,*}, Fail Sultanov ^{1,2,*}, Renat Beissenov ^{3,4,*}, Arman Umirzakov ⁴, Almaz Mereke ⁴, Askhat Bekbaev ^{5,*} and Igor Chuprakov ^{6,7}

¹ Faculty of Chemistry and Chemical Technology, al-Farabi Kazakh National University, Almaty 050000, Kazakhstan; baglan.bakbolat@mail.ru

² Laboratory of Energy-Intensive and Nanomaterials, Institute of Combustion Problems, Almaty 050000, Kazakhstan

³ Department of Engineering Physics, Satbayev University, Almaty 050013, Kazakhstan

⁴ Laboratory of EPR Spectroscopy Named after Y.V. Gorelkin, LLP "Institute of Physics and Technology", Almaty 050032, Kazakhstan; arman_umirzakov@mail.ru (A.U.); mereke.almaz@mail.ru (A.M.)

⁵ Faculty of Physics and Technology, al-Farabi Kazakh National University, Almaty 050000, Kazakhstan

⁶ Frank Laboratory of Neutron Physics, Joint Institute for Nuclear Research (JINR), Dubna 141980, Russia; chupa@nf.jinr.ru

⁷ Faculty of Physics and Technical Sciences, L.N. Gumilyov Eurasian National University, Astana 010000, Kazakhstan

* Correspondence: chingis.daulbayev@kaznu.kz (C.D.); sultanov.fail@kaznu.kz (F.S.); r.beissenov@satbayev.university (R.B.); bekbaev.ashat2@kaznu.kz (A.B.)

Received: 7 August 2020; Accepted: 29 August 2020; Published: 9 September 2020



Abstract: The growth of industrialization, which is forced to use non-renewable energy sources, leads to an increase in environmental pollution. Therefore, it is necessary not only to reduce the use of fossil fuels to meet energy needs but also to replace it with cleaner fuels. Production of hydrogen by splitting water is considered one of the most promising ways to use solar energy. TiO₂ is an amphoteric oxide that occurs naturally in several modifications. This review summarizes recent advances of doped TiO₂-based photocatalysts used in hydrogen production and the degradation of organic pollutants in water. An intense scientific and practical interest in these processes is aroused by the fact that they aim to solve global problems of energy conservation and ecology.

Keywords: titanium dioxide; photocatalysis; hydrogen evolution; photodegradation

1. Introduction

At present, hydrogen is regarded as the fuel of the future. Compared to carbon fuel, hydrogen is considered a renewable and environmentally friendly source of energy. There are various methods for producing hydrogen on an industrial scale. However, all known methods are characterized by high energy consumption, which makes the process of hydrogen production on a large scale disadvantageous. The production of hydrogen by photocatalytic water splitting is technologically simple, and the outcoming gases are environmentally friendly.

TiO₂ is a wide-bandgap semiconductor. In nature, TiO₂ is usually found in three different crystalline structures: rutile, anatase, and brookite. TiO₂ in anatase form is the most widespread photocatalyst for hydrogen evolution [1]. However, it cannot be used in the spectrum of visible light, since its bandgap (E_g) for different crystalline phases (anatase—3.2 eV, rutile—3.0 eV, and brookite—3.3 eV) is in the UV region. Also, the efficiency of photocatalysis in addition to the bandgap depends on

many other factors [2]. In the 1970s, Fujishima and Honda studied the photoelectrochemical splitting of water, where a TiO₂-based electrode demonstrated the ability to split water under the influence of ultraviolet radiation [3]. Photocatalysis is a complex reaction consisting of the processes starting from light absorption to generate charge carriers up to surface catalytic reactions due to which gas is formed (Figure 1). This process only requires a photocatalyst (TiO₂), which is not consumed during the entire process, water, sunlight or ultraviolet radiation. During the absorption of light ($\geq E_g$) by the photocatalyst, an excited electron (e_{CB}^-) transfers from the valence band into the conduction band. This transition of the electron leads to the generation of a positively charged carrier-hole (h_{VB}^+) in the valence band (Equation (1)). Also, these charge carriers can recombine among themselves (Equation (2)) [4,5].

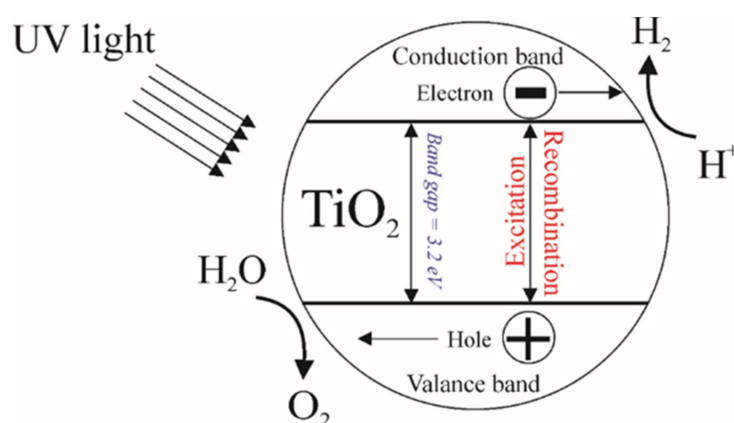


Figure 1. The mechanism of photocatalytic water splitting on TiO₂ based photocatalyst.

Another important application of TiO₂-based photocatalysts is based on their ability to discolor and completely decompose organic dyes contained in water. In addition, there are a number of works in which TiO₂-based photocatalysts were used to neutralize harmful to the atmosphere gases [6–9]. Chemical stability, easy accessibility, nontoxicity and the ability to oxidize under the influence of radiation, allow TiO₂-based photocatalysts to solve the main global problems associated with pollution of the environment and need for renewable energy [10,11]. Currently, TiO₂ as a photocatalyst is commercially produced in powder form. The most common brand of TiO₂ based photocatalyst are P-25 Degussa/Evonik, TiO₂ nanofibers from Kertak, TiO₂ Millennium PC-500, TiO₂ Hombikat UV-100, Sigma Aldrich TiO₂, TiO₂ PK-10, and P90 Aeroxide.

This paper aims to provide a brief overview of articles published starting from 2017 on new research and developments of TiO₂ based photocatalysts with significant advances. In this review, attention is also paid to the study on the mechanism of photocatalytic processes, factors affecting the activity of photocatalysts, and new techniques used to increase the activity of TiO₂ based photocatalysts during the splitting of water with the evolution of hydrogen and decomposition of organic compounds utilized for water purification.

2. Factors Affecting the Efficiency of Photocatalysis and Techniques Used to Improve the Efficiency of TiO₂-Based Photocatalysts

2.1. Lifetime of Photogenerated Charge Carriers

The activity of photocatalysts strongly depends on the lifetime of photogenerated electron-hole pairs. An important role is played by the rate at which charge carriers can reach the surface of

the photocatalysts. The results of spectroscopic studies show that the time intervals between redox reactions or recombination involving charge carriers are extremely short, resulting in a significant reduction of the photocatalytic activity of TiO_2 . In the case of recombination of charge carriers in a sufficiently fast interval (<0.1 ns), the photocatalytic activity of the semiconductor is not observed. For example, the lifetime of electron-hole pairs of ~ 250 ns (TiO_2) is considered relatively long [12]. Thus, it can be concluded that a high recombination rate and barriers, that prevent the transfer of charge carriers to the semiconductor surface, reduce photoactivity, despite the high concentration of initially photogenerated pairs. In this regard, to avoid their recombination, it becomes necessary to use cocatalysts in order to increase the lifetimes of electrons and holes.

2.2. The Particle Size of Photocatalyst

Compared to microparticles, TiO_2 nanoparticles have, generally, a higher photocatalytic activity [13,14]. This is due to the small diameter of the nanoparticles, in which the charge requires minimal effort to transfer to the surface. If the particle size decreases, the distance that photogenerated electrons and holes need to travel to the surface where the reactions take place is reduced, thereby reducing the probability of recombination. For TiO_2 photocatalyst microparticles, the penetration depth of UV rays is limited and amounts to about ~ 100 nm. This means that the inner part of the TiO_2 photocatalyst microparticle remains in a passive state. [15]. Figure 2 shows the scheme of light absorption by nano- and microparticles of TiO_2 . This is one of the reasons for the increased interest in nanosized particles of TiO_2 .

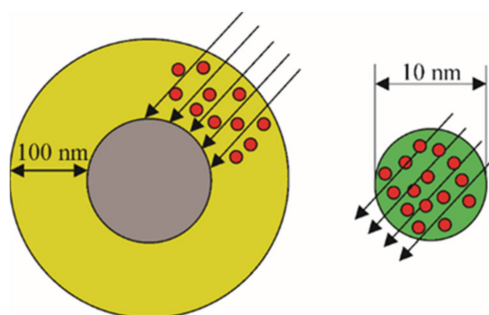


Figure 2. Light absorption by micro- and nanoparticles of TiO_2 .

As shown in Figure 2, a decrease in the particle size of the photocatalyst to nanoscale facilitates the absorption of light by the entire volume of particles. However, there is a limitation regarding the minimum sizes to which it is desirable to reduce the particles of the photocatalyst, due to the onset of quantum effects. They become significant at particle sizes less than 2 nm for both anatase and rutile, and finally, this leads to a change in the bandgap. An increase in the size of the photocatalyst crystals leads to a decrease in the recombination of the electron-hole pair at the defects of the crystal lattice and to an increase in photocatalytic activity. For example, in [16], nanoparticles with a size of 25 nm were found to be more productive than nanoparticles of 15 nm. On the other hand, the bandgap is directly proportional to the size of the photocatalyst crystals. That is why it is necessary to find the optimal crystal size of TiO_2 and control it in the process of its obtaining.

To increase the photoactivity of TiO_2 in the visible region of the spectrum, the spectral region of its absorption should be expanded. There are several approaches for sensitizing TiO_2 to visible light: doping with cationic and anionic elements or metal nanoparticles. Elements of the 3d- and 2p-groups are often used as additives to reduce the value of the bandgap of the photocatalyst [17,18].

2.3. Doping with Cations

The essence of cationic doping is the introduction of metal cations into the crystal structure of TiO_2 at the position of Ti^{4+} ions. Rare-earth, noble, and transition metal cations can be used [19]. Doping

with cations significantly expands the absorption spectrum of TiO₂, increases the redox potential of the formed radicals, and increases quantum efficiency by reducing the degree of recombination of electrons and holes. The nature and concentration of the dopant change the charge distribution on the TiO₂ surface and affects the process of photo corrosion and photocatalytic activity [20]. However, an increase in the absorption of visible light does not always lead to an increase in the activity of the photocatalyst. As a result of doping with cations, a certain number of defects appear in the TiO₂ structure, which can act as charge recombination centers, this leading to a decrease in photocatalytic activity even under the influence of UV light.

In [21], Kryzhitsky et al. show the change in the activity of photocatalytic properties of rutile and anatase forms of nanocrystalline TiO₂ depending on the nature of metal-based dopants. According to the results of the study, it is found that doping does not significantly change the bandgap of rutile, while in the case of doping anatase with iron and chromium, its bandgap narrows significantly. As a result of doping with metals, the photocatalytic activity of anatase (A) increases in the following order: A < A/Co < A/Cu < A/Fe. In the case of rutile (R), its photocatalytic activity decreases in the following order: R > R/Co > R/Cu > R/Fe > R/Cr. According to the authors, the decrease in the photoactivity of TiO₂ may be associated with the inhibitory effect of impurity cations.

2.4. Doping with Anionic Elements

Over the past few years, it has been shown that TiO₂ samples doped with nonmetallic elements (nitrogen, carbon, sulfur, boron, phosphorus, and fluorine) in the anionic positions of TiO₂, demonstrate high photoactivity in the UV and visible regions of the solar spectrum [22,23]. Among all the anions, carbon, nitrogen, and fluorine caused the most significant interest [24–26]. The substitution of oxygen atoms to carbon leads to the formation of new levels (C2p) above the ceiling of the valence band of TiO₂ (O2p), which reduces the bandgap and shifts the absorption spectrum. The inclusion of carbon in TiO₂ can also lead to the formation of carbon compounds on the surface of the photocatalyst, which acts as absorption centers of visible radiation [27].

Doping with nitrogen atoms is the most popular way to improve the photocatalytic performance of TiO₂. Introduction of nitrogen into the TiO₂ structure contributes to a significant shift of the absorption spectrum into the visible region of the solar spectrum, a change in the refractive index, an increase in hardness, electrical conductivity, elastic modulus, and photocatalytic activity in regard to visible light [28,29]. Upon substitution of anions, a new level is formed above the valence band of TiO₂ [30]. As shown in Figure 3, the presence of nitrogen leads to a change of the bandgap $E_{g1}(\text{TiO}_2) > E_{g2}(\text{N-doped TiO}_2)$, thus contributing to the absorption of photons of light with lower energy.

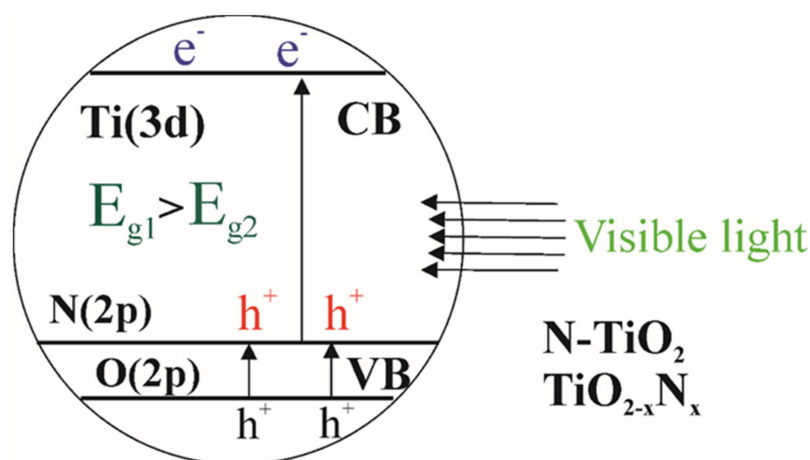


Figure 3. Changes in the band gap of TiO₂ upon doping with nitrogen atoms.

Doping with nitrogen in the oxygen position is difficult since the ionic radius of nitrogen (1.71 Å) is much larger than that for oxygen (1.4 Å). Another auspicious element in the anionic positions of TiO₂ is fluorine atoms [31]. Unlike nitrogen, fluorine atoms easily replace oxygen due to the close ion radius (1.33 Å for F⁻ and 1.4 Å for O²⁻). The increase in photocatalytic activity is mainly associated with an improvement in the degree of crystallinity of TiO₂ due to doping with fluorine [32]. It has been determined that crystallinity and the specific surface area also affect the photoactivity of TiO₂ [33,34]. The crystalline modification of TiO₂ in comparison with amorphous TiO₂ has significantly fewer defects, which reduce the possibility of recombination processes and contributes to the efficient movement of photogenerated charge carriers in the semiconductor. Since redox reactions occur on the surface of TiO₂, one of the main requirements for photocatalysts is the presence of a developed specific surface area. However, the presence of a developed specific surface area implies a large number of defects in the structure and a low degree of crystallinity and, as a result, reduces photocatalytic activity. Therefore, to increase photocatalytic activity, it is important to find a balance between the above factors.

2.5. Doping/Loading with Metal Nanoparticles

The application of metal nanoparticles is another alternative approach to the modification of photocatalysts. A review of the recent literature shows that metals (Co, Pt, Ag, Au, Pd, Ni, Cu, Eu, Fe, etc.) significantly increase the photocatalytic activity of TiO₂ [35–37]. The low location of the Fermi level of these metals compared to TiO₂ can lead to the movement of electrons from the TiO₂ structure to metal particles deposited on its surface. This helps to avoid the recombination of charge carriers, since the holes remain in the valence band of TiO₂. This is also beneficial for avoiding the recombination of charge carriers since the holes remain in the valence band of TiO₂. A number of conducted investigations indicate that the properties of these photocatalysts depend on the dispersion of metal particles [38,39]. Enhanced photocatalytic properties of metals appear when their size decreases <2.0 nm [40]. Despite the foregoing, too high concentration of metal particles can block the surface of TiO₂ and prevent the absorption of photons, leading to a decrease in the efficiency of the photocatalyst.

3. The Utilization of Photocatalysts Based on TiO₂

3.1. Hydrogen Evolution

Hydrogen can be produced by using nanoscale TiO₂ based photocatalysts with various morphologies in the form of nanowires, nanospheres, nanorods, nanotubes, and nanosheets [41]. Table 1 lists some TiO₂ nanocomposites with different structures, as well as their photocatalytic characteristics.

Table 1. TiO₂-based photocatalysts with different structures utilized for hydrogen evolution under splitting water mixtures.

Photocatalyst	Structure	Light Source	Sacrificial Agents	Evolution H ₂	Ref.
Au/TiO ₂ Pt/TiO ₂	microspheres	15 W fluorescent tubes (λ _{max} = 365 nm)	25% vol. methanol	1118 μmol h ⁻¹ 2125 μmol h ⁻¹	[42]
TiO ₂	nanofibers	300 W Xenon lamp	10% vol. methanol	3200 μmol h ⁻¹ g ⁻¹	[43]
Cu/TiO ₂	nanorods	300 W Xe lamp (λ > 300 nm)	20% vol. methanol	1023.8 μmol h ⁻¹	[44]
TiO ₂ /WO ₃ /Au	nanofibers	300 W Xe arc lamp	35% vol. methanol	269.63 μmol h ⁻¹	[45]
M/TiO ₂ /rGO M = Au or Pt	nanoparticles	300 W Xenon lamp (λ > 300 nm)	20% vol. methanol	670 μmol h ⁻¹	[46]
MoSe ₂ /TiO ₂	nanoparticles	Xe arc lamp (PLS-SXE300)	10% vol. methanol	4.9 μmol h ⁻¹	[47]
BCN-TiO ₂	nanosheets & nanoparticles	300 W xenon lamp with a UV-cutoff filter (λ ≥ 420 nm)	20% vol. triethanolamine	68.54 μmol h ⁻¹ g ⁻¹	[48]
TiO ₂ /C ₃ N ₄	double-shell microtubes	300 W xenon lamp	20% vol. methanol	10.1 mmol h ⁻¹ g ⁻¹	[49]
ZnS@g-C ₃ N ₄ /TiO ₂	nanospheres	300 W Xenon lamp (λ > 400 nm)	10% vol. triethanolamine	422 μmol h ⁻¹ g ⁻¹	[50]

P. Melián et al. [42] demonstrated that loading of nanosized TiO₂ microspheres with Au and Pt metals increases the hydrogen evolution twice. In the case of using Au, the maximum hydrogen

evolution was determined at 1.5 wt.% content of Au in the sample with the yield of hydrogen $1118 \mu\text{mol h}^{-1}$, while for Pt its optimal content in the sample was 0.27 wt.% with the yield of hydrogen $2125 \mu\text{mol h}^{-1}$. The excess of dopants may result in decrease of photocatalyst activity due to possible complete coverage of TiO_2 surface, thus, hindering the light to be absorbed. A literature review also showed that the difference in the optimal ratio for each metal could be associated with the formation of recombination centers on the semiconductor surface by metal particles [51,52].

A positive effect on the rate of H_2 production was found when using sacrificial agents acting as electron donors (hole scavengers) during photoreforming, in which the hydroxyl radical is consumed by the sacrificial agents. In general, there are two types of sacrificial reagents: organic and inorganic based electron donors. Among organic electron donors, the most effective are water–alcohol mixtures, in particular, methanol > ethanol > ethylene glycol > glycerol [53–59]. However, an increase in the concentration of the sacrificial agent does not always lead to an increase in the yield of hydrogen. Y.-K. Park et al. [60] showed that the rate of hydrogen evolution also increases depending on the concentration of methanol (Figure 4a). At low concentrations, the rate of hydrogen formation in solutions is proportional to the concentration of methanol, while at higher concentrations, it approaches to a constant value [61]. Nevertheless, after adding a certain amount of methanol and ethanol, a further increase in its concentration leads to a decrease in the rate of hydrogen evolution (Figure 4b). The yield of hydrogen during photoreforming has a maximum output during 80–90 min and after it decreases. This is due to the formation of a significant amount of methane and ethane, during which photogenerated electrons (e_{CB}^-) and holes (h_{VB}^+) are consumed [54].

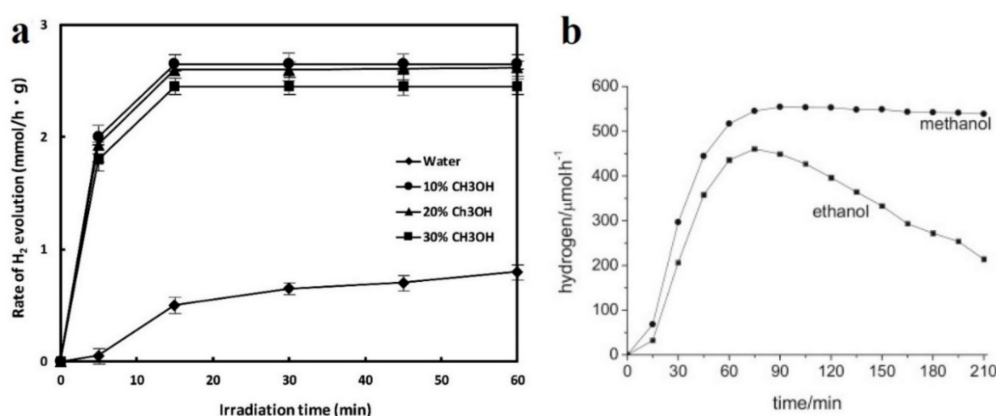


Figure 4. (a) Rate of hydrogen evolution from photocatalysis of aqueous methanol solution on Ag/TiO_2 photocatalysts. This figure is reprinted from [60], with permission from Elsevier, 2020; (b) H_2 production patterns for 24.47 M (100% v/v) of methanol and 17.06 M (100% v/v) of ethanol. This figure is reprinted from [54], with permission from Elsevier, 2015.

The amount of dopant also has a significant effect on the efficiency of light absorption by the photocatalyst and on its photocatalytic activity. For example, Udayabhanu et al. [62] prepared $\text{Cu-TiO}_2/\text{CuO}$ nanocomposites containing different amount of Cu. The color of the obtained samples, depending on the concentration of $\text{Cu-TiO}_2/\text{CuO}$ (CUT) from 1 to 4 mol% (the samples were as named CUT 1, CUT 2, CUT 3, and CUT 4) changes from light green to dark green (Figure 5). To evaluate the photocatalytic activity of hydrogen production, scientists compared the activities of obtained nanocomposites with conventional TiO_2 . Sunlight was used as the source of radiation, and glycerol was chosen as a sacrificial agent. According to the results, the CUT 3 sample based on $\text{Cu-TiO}_2/\text{CuO}$ possessed the highest yield of hydrogen ($10.453 \mu\text{mol h}^{-1} \text{g}^{-1}$ of H_2 under sunlight and $4.714 \mu\text{mol h}^{-1} \text{g}^{-1}$ of H_2 under visible light). Nevertheless, this type of photocatalyst is effective only for hydrogen production, since it has shown low efficiency in the decomposition of organic dye and metal detoxification in water.



Figure 5. Colour of synthesized pristine and Cu-TiO₂/CuO composite nanopowders. This figure is reprinted from [62], with permission from Elsevier, 2020.

The photocatalyst efficiency is affected not only by the nature of the alloying element but also by its concentration. For example, X. Xing et al. in [63] demonstrated the dependence of the yield of hydrogen on the light intensity and the concentration of the dopant. From Figure 6a, it is clear that the increase of concentrations of each photocatalyst (pure TiO₂ and Au/TiO₂) results in increase of the rate of hydrogen production. However, the hydrogen generation rate for Au/TiO₂ photocatalyst at the same light intensity is 18–21 times higher than that for pure TiO₂. The explanation to this is that Au can limit charge carriers' recombinations and, what is more, the visible light absorption of photocatalyst is enhanced by the localized surface plasmon resonance effect of Au nanosized particles. The influence of the light intensity (from 1 to 9 kW/m²) and the duration of exposure on the rate of hydrogen generation for Au/TiO₂ nanoparticles with a concentration of 1 g/L is also shown in Figure 6b.

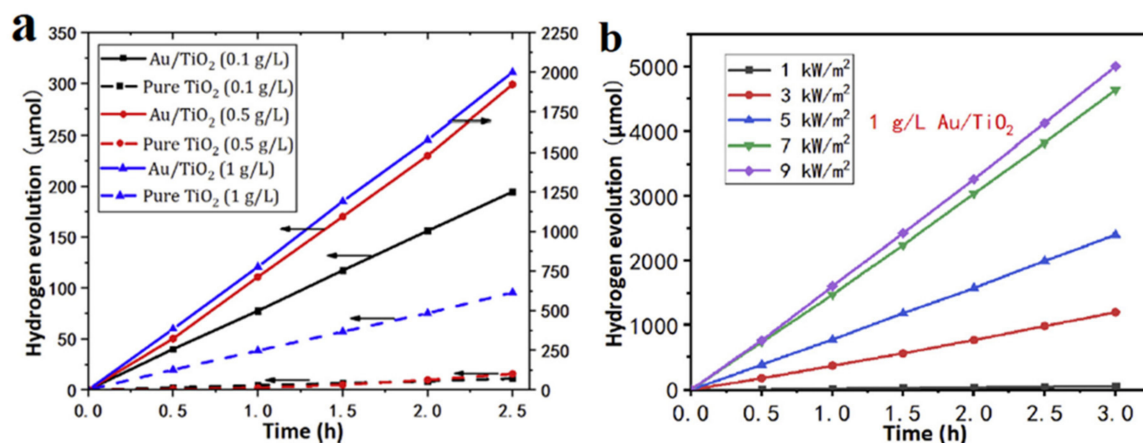


Figure 6. (a) Hydrogen evolution of pure TiO₂ nanoparticles and Au/TiO₂ nanoparticles at the same light intensity of 5 kW/m²; (b) Hydrogen evolution in 1–9 kW/m² light intensities of 1 g/L Au/TiO₂ solutions. Both figures are reprinted from [63], with permission from Elsevier, 2020.

The photocatalytic properties of the material can be improved by creating composites based on different photocatalysts. For example, E.-C. Su et al. [64] obtained a composite photocatalyst based on Pt/N-TiO₂/SrTiO₃-TiO₂ in the form of nanotubes using a two-stage hydrothermal process (SrTiO₃ is also a photocatalyst with a bandgap of 3.2 eV with a perovskite-type structure [65]). The obtained results showed that this composite photocatalyst is able to operate under sunlight with the rate of hydrogen evolution up to 3873 μmol/h/g.

In practice, photocatalytic reactions are mainly carried out at room temperature. It is found that increasing temperature has a positive effect on the activity of some photocatalysts, which makes it relevant to develop new photocatalysts based on the anatase form of TiO₂ with a thermostable phase.

3.2. Photodegradation

Organic dyes are used on a large scale in modern industries. Wastewater polluted with such substances subsequently leads to environmental problems [66,67]. This is due to the fact that most

organic dyes consist of biodegradable aromatic structures and azo-groups. Adsorption and catalytic oxidation remain the most effective among the methods for treating wastewater from dyes [68–70]. For photocatalytic degradation of organic compounds, in most cases, TiO₂, in the doped form, is used.

Graphene has a large specific surface area and electrical conductivity. The presence of such properties in graphene is of interest to scientists in the preparation of a graphene/nano-TiO₂-based photocatalyst [71–73]. After irradiation of a TiO₂-based photocatalyst, electrons move into the graphene structure. Based on the author's results [74], it helps to avoid recombination between charge carriers. TiO₂/graphene-based photocatalyst can be obtained by creating either a chemical bond between them or via the approach of their mechanically mixing [75,76]. Due to existence of chemical bond, the electron is transferred unhindered from the photocatalyst to graphene, reducing the probability of recombination. This is the main explanation for the increased activity of the photocatalyst with graphene.

Composites based on TiO₂/graphene attract scientists' attention not only as highly efficient photocatalysts due to light absorption in a wide range and charge separation, but also taking in account its high adsorption capacity to pollutants. However, TiO₂/graphene-based composite produced by the hydrothermal method cannot serve as an effective photocatalyst. The reason is the agglomeration of graphene layers, which adversely affects the adsorption and photocatalytic properties. The solution to this problem is described in [77], where graphene-based aerogel was used as an auxiliary material for TiO₂ [78,79]. Aerogel was obtained by thermal reduction of graphene oxide. Table 2 lists some reports on the use of composite TiO₂/graphene based photocatalysts to remove various organic compounds (pollutants and dyes) from water.

Table 2. Removal percentage of some organic pollutants by TiO₂/graphene based photocatalysts.

Photocatalyst	Organic Pollutant	Light Source	Irradiation Time	Efficiency	Ref.
TiO ₂ @rGO	2,4,6 trichlorophenol	Mercury lamp (11 W)	180 min	90%	[80]
TiO ₂ /Fe ₃ O ₄ /GO	Methylene blue	Halogen lamp (500 W)	90 min	76%	[81]
GO/TiO ₂ nanotubes	Perfluorooctanoic acid	UV lamp (8 W)	240 min	97%	[82]
N-TiO ₂ /Ag ₃ PO ₄ @GO	Acid Blue 25	Halogen bulb (250 W)	20 min	98%	[83]
Ag and rGO modified TiO ₂	Tetrabromobisphenol A	Xenon light (500 W)	80 min	99.6%	[84]
N-doped graphene/TiO ₂	Bisphenol A	Mercury lamp (300 W)	60 min	100%	[85]
3D polyaniline/TiO ₂ /rGO hydrogel	BPA	Mercury lamp (500 W)	40 min	100%	[86]

Before testing photocatalytic activity, it was necessary to saturate the materials in the dark conditions. If saturation is not performed at dark conditions, a decrease in the concentration of the target pollutant or the color intensity change of the used in experiment dye will be associated not only with photocatalysis, but also with adsorption and photocatalytic degradation, so the effectiveness of the photocatalyst will be incorrect. X. Sun et al. [77] compared two samples of a photocatalyst of the same mass: hydrothermally obtained TiO₂-reduced graphene oxide (rGO), and aerogel based on TiO₂-rGO (Figure 7a). As can be seen, despite the equal mass of both samples, the TiO₂-rGO based aerogel has a larger specific volume than that of the second sample. For further characterization of their adsorption, both samples were used to adsorb methylene blue in the dark. During the experiment, the absorption intensity was analyzed. The results showed that it took 2 min for TiO₂-rGO based aerogel to achieve adsorption saturation, while for TiO₂-rGO powder, it took more than 10 min (Figure 7b). Figure 7c,d demonstrates the color change of methylene blue, which proves the high absorption coefficient of visible light by TiO₂-rGO aerogels. According to the authors, the adsorption rate also affects the efficiency of photocatalysts.

Photocatalytic activity directly depends on the number of active centers on the surface of the photocatalyst. Photolithography is a block of technological processes of photochemical technology aimed at creating the relief in the film, as well as a film of metal deposited on a substrate [87,88]. Using this method, a group of scientists [89] managed to obtain TiO₂ films with lattice, square, and hexagonal structures (Figure 8) and investigate the influence of a such surface textures on the photocatalysis. Obtained results showed that the activity of photocatalyst in the form of a film is not improved by

increasing the values of specific surface area. Surface texture also has an effect on mass transfer during photocatalysis.

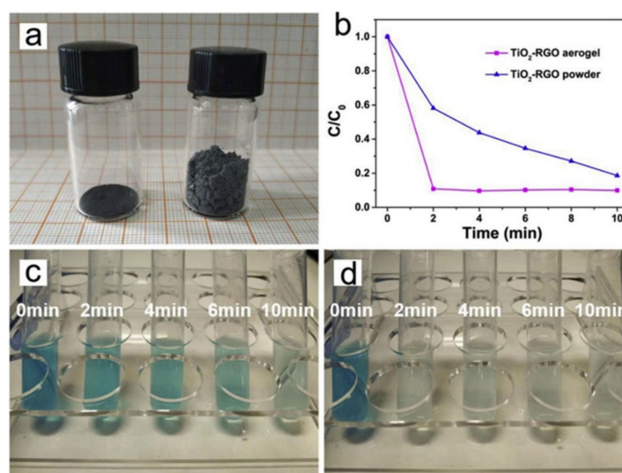


Figure 7. (a) Photograph of 80 mg TiO₂-reduced graphene oxide (rGO) powder (left) and aerogel (right); (b) methylene blue (MB) dark adsorption results of the TiO₂-rGO aerogel/powder; color changing of MB solution during dark adsorption with TiO₂-rGO powder (c), and aerogel (d). All figures are reprinted from [77], with permission from Elsevier, 2020.

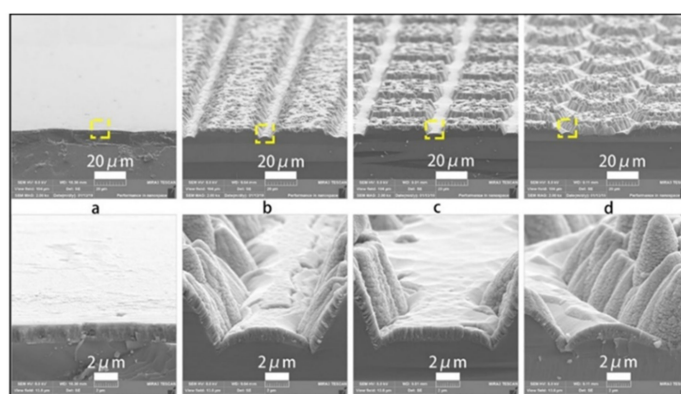


Figure 8. SEM images of (a) planar TiO₂ film; (b) grating-structured TiO₂ film; (c) square-structured TiO₂ film; (d) hexagon-structured TiO₂ film. All figures are reprinted from [89], with permission from Elsevier, 2019.

To evaluate the activity of photocatalysts, scientists conducted an experiment, in which the dye degradation occurred in water as a result of its exposure with UV (254 nm) on methyl orange. As shown in Figure 9, the microstructured TiO₂ films exhibit a more active photocatalytic activity than TiO₂ films with a flat surface. According to scientists, this is due to the presence of reaction centers on the surface of microstructured films. The highest photocatalytic activity was observed for TiO₂ films with a square microstructure. The experimental results showed that the efficiency of photocatalysts is influenced not only by the surface area, but also by the type of their microstructure. It was revealed, that the TiO₂ film with a grating structure, despite its low specific surface area, possessed photoactive properties similar to the TiO₂ film with a hexagonal structure [89].

A significant role during photocatalysis is played by the surface microstructure, which influences the mass transfer of degradable organic compounds by the diffusion to the surface of the photocatalyst. It is important to take into account the fact that the fluid flowing over the surface with protrusions meets more resistance from the side of the walls, compared to the fluid flowing through the flat surface. As a result, such protrusions can adversely affect the degradation efficiency of organic pollutants.

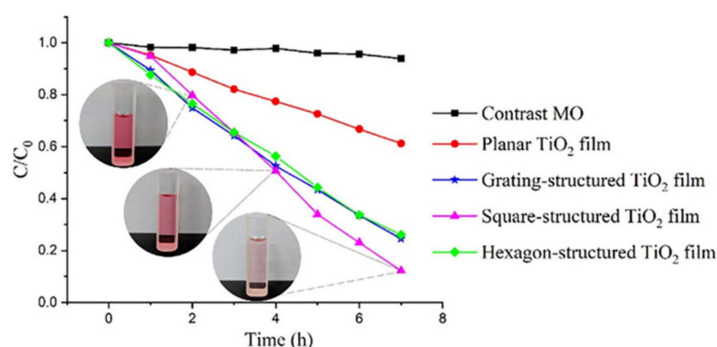


Figure 9. Photocatalytic degradation of MO under ultraviolet light (254 nm) irradiation. C and C_0 represent the real-time and initial concentration of methyl orange solution. This figure is reprinted from [89], with permission from Elsevier, 2019.

TiO₂ doped with Fe₂O₃ is one of the best-known effective photocatalysts. Due to the narrow bandgap of Fe₂O₃ (2.2 eV), its doping leads to a redshift of the light response of the photocatalyst. The phenomenon of decreasing of photoactivity of TiO₂ based photocatalyst doped with non-metals during heating, the high cost of some metals and the availability of Fe₂O₃ in large quantities increases the attractiveness of Fe₂O₃ over other dopants [90]. J.-J. Zhang et al. [91] used Fe₂O₃ nanoparticles, which served as a doping agent for obtaining the TiO₂/graphene aerogel (GA) based photocatalyst with a 3D structure (Figure 10). Due to the narrow bandgap (2.0 eV), Fe₂O₃ can easily generate electron-hole pairs, thereby contributing to the photodegradation of rhodamine B even in visible light. The results showed that the aqueous solution containing rhodamine B (RhB) was purified to 97.7% (Figure 10 b). Fe₃O₄ can also be used as a doping agent for the photocatalysis [92]. For example, F. Soltani-Nezhad et al. [93] presented a method for producing a GO/Fe₃O₄/TiO₂-NiO-based photocatalyst, which is able to efficiently degrade imidacloprid (pesticide).

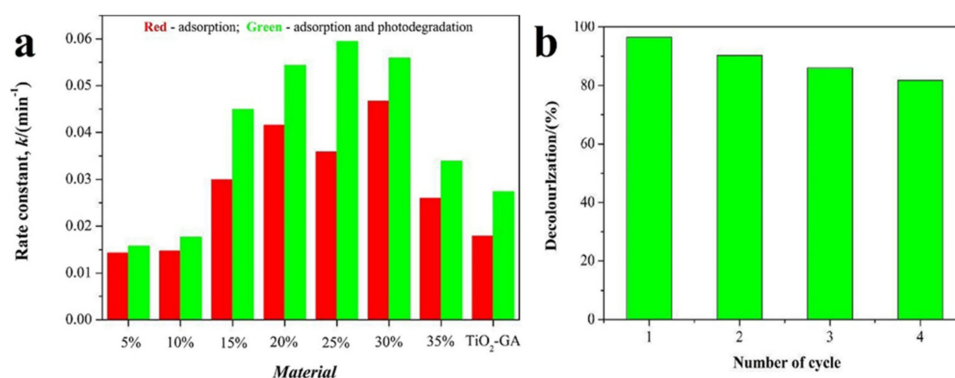


Figure 10. (a) The rate constants for the adsorption and the collective removal of rhodamine B (RhB) over TiO₂-GA and the Fe₂O₃-TiO₂-GA composites; (b) stability of the Fe₂O₃-TiO₂-GA (25%) composites in the removal of RhB dye. Both figures are reprinted from [91], with permission from Elsevier, 2018.

To increase the efficiency of the process of degradation of organic pollutants by photocatalysis, attempts have been made to combine radiation with ultrasonic cavitation. S. Rajoriya et al. [94] reported the photodegradation of 4-acetamidophenol to 91% using Sm (samarium) and N-doped TiO₂ photocatalysts, in which a combination of UV radiation, hydrodynamic cavitation, and ultrasound was applied. In another work, the use of N and Cu-doped TiO₂@CNTs in sono-photocatalysis for purification of pharmaceutical wastewater is discussed [95]. The results showed that when using a commercial Xe lamp (50 W) and ultrasound for pharmaceutical wastewaters treatment, the photocatalyst removal efficiency within 180 min were 100, 93, and 89% for sulfamethoxazole, chemical oxygen demand, and total organic carbon, respectively.

The great interest in the use of ultrasonic action during photocatalysis is justified by the enhancement of electronic excitations, which leads to an increase in the density of pairs of charged particles. Under the influence of ultrasound, the aggregate photocatalysts are dispersed, contributing to the rapid renewal and expansion of the boundaries of heterogeneous reactions, which improves the mass transfer and the course of chemical reactions [96,97].

4. Conclusions

In this review, information on the main mechanisms of water splitting and decomposition of organic compounds by TiO₂-based photocatalysts was collected and analyzed. The efficiency of TiO₂ doping by various components, which significantly increases the photocatalytic activity, is shown. In addition, other factors, such as the bandgap, charge carrier recombination, the use of sacrificial agents, the size and type of photocatalyst structures, surface morphology, photocatalyst concentration in solution, radiation source power, etc., which can affect the photocatalysis were analyzed. Despite the reports of scientists on the development of effective photocatalysts capable of operating under sunlight, their use is still not economically viable. Therefore, due to the growth of environmental problems and the limited availability of hydrocarbon fuels, investigations in the field of hydrogen production by “artificial photosynthesis” will undoubtedly increase.

Author Contributions: Conceptualization, B.B. and C.D.; writing—original draft preparation, F.S., R.B., A.B., I.C. and B.B.; writing—review and editing, A.U. and A.M.; project administration, R.B. All authors have read and agreed to the published version of the manuscript.

Funding: This study was funded by Ministry of Education and Science of the Republic of Kazakhstan № AP05135273. The name of the focal area of the development of science, on which the application is submitted: Energy and Machine industry. The name of the specialized research area, on which the application is filed, type of study: Alternative energy and technology: renewable energy sources, nuclear and hydrogen energy, other energy sources, applied research.

Acknowledgments: Askhat Bekbaev is grateful to al-Farabi Kazakh National University for financial support in the frame of the postdoctoral fellowship program.

Conflicts of Interest: The authors declare no conflict of interest.

References

1. Samokhvalov, A. Hydrogen by photocatalysis with nitrogen codoped titanium dioxide. *Renew. Sustain. Energy Rev.* **2017**, *72*, 981–1000. [[CrossRef](#)]
2. Phoon, B.L.; Lai, C.W.; Juan, J.C.; Show, P.-L.; Pan, G.-T. Recent developments of strontium titanate for photocatalytic water splitting application. *Int. J. Hydrogen Energy* **2019**, *44*, 14316–14340. [[CrossRef](#)]
3. Fujishima, A.; Honda, K. Electrochemical Photolysis of Water at a Semiconductor Electrode. *Nature* **1972**, *238*, 37–38. [[CrossRef](#)] [[PubMed](#)]
4. Xiao, N.; Li, S.; Li, X.; Ge, L.; Gao, Y.; Li, N. The roles and mechanism of cocatalysts in photocatalytic water splitting to produce hydrogen. *Chin. J. Catal.* **2020**, *41*, 642–671. [[CrossRef](#)]
5. Katal, R.; Masudy-Panah, S.; Tanhaei, M.; Farahani, M.H.; Jianguyong, H. A review on the synthesis of the various types of anatase TiO₂ facets and their applications for photocatalysis. *Chem. Eng. J.* **2020**, *384*, 123384. [[CrossRef](#)]
6. Bingham, M.; Mills, A. Photonic efficiency and selectivity study of M (M = Pt, Pd, Au and Ag)/TiO₂ photocatalysts for methanol reforming in the gas phase. *J. Photochem. Photobiol. A Chem.* **2020**, *389*, 112257. [[CrossRef](#)]
7. Paz, Y. Application of TiO₂ photocatalysis for air treatment: Patents’ overview. *Appl. Catal. B Environ.* **2010**, *99*, 448–460. [[CrossRef](#)]
8. Shayegan, Z.; Lee, C.-S.; Haghighat, F. TiO₂ photocatalyst for removal of volatile organic compounds in gas phase—A review. *Chem. Eng. J.* **2018**, *334*, 2408–2439. [[CrossRef](#)]
9. Verbruggen, S.W. TiO₂ photocatalysis for the degradation of pollutants in gas phase: From morphological design to plasmonic enhancement. *J. Photochem. Photobiol. C Photochem. Rev.* **2015**, *24*, 64–82. [[CrossRef](#)]

10. Kou, J.; Lu, C.; Wang, J.; Chen, Y.; Xu, Z.; Varma, R.S. Selectivity Enhancement in Heterogeneous Photocatalytic Transformations. *Chem. Rev.* **2017**, *117*, 1445–1514. [[CrossRef](#)]
11. Parrino, F.; Bellardita, M.; García-López, E.I.; Marci, G.; Loddo, V.; Palmisano, L. Heterogeneous Photocatalysis for Selective Formation of High-Value-Added Molecules: Some Chemical and Engineering Aspects. *ACS Catal.* **2018**, *8*, 11191–11225. [[CrossRef](#)]
12. Yang, Q.; Dong, L.; Su, R.; Hu, B.; Wang, Z.; Jin, Y.; Wang, Y.; Besenbacher, F.; Dong, M. Nanostructured heterogeneous photo-catalysts for hydrogen production and water splitting: A comprehensive insight. *Appl. Mater. Today* **2019**, *17*, 159–182. [[CrossRef](#)]
13. Vajda, K.; Saszet, K.; Kedves, E.Z.; Kása, Z.; Danciu, V.; Baia, L.; Magyari, K.; Hernádi, K.; Kovács, G.; Pap, Z. Shape-controlled agglomeration of TiO₂ nanoparticles. New insights on polycrystallinity vs. single crystals in photocatalysis. *Ceram. Int.* **2016**, *42*, 3077–3087. [[CrossRef](#)]
14. Li, D.; Song, H.; Meng, X.; Shen, T.; Sun, J.; Han, W.; Wang, X. Effects of Particle Size on the Structure and Photocatalytic Performance by Alkali-Treated TiO₂. *Nanomaterials* **2020**, *10*, 546. [[CrossRef](#)] [[PubMed](#)]
15. Nagaraj, G.; Irudayaraj, A.; Josephine, R.L. Tuning the optical band Gap of pure TiO₂ via photon induced method. *Optik* **2019**, *179*, 889–894.
16. Allen, N.S.; Vishnyakov, V.; Kelly, P.J.; Kriek, R.J.; Mahdjoub, N.; Hill, C. Characterisation and photocatalytic assessment of TiO₂ nano-polymorphs: Influence of crystallite size and influence of thermal treatment on paint coatings and dye fading kinetics. *J. Phys. Chem. Solids* **2019**, *126*, 131–142. [[CrossRef](#)]
17. Sinhmar, A.; Setia, H.; Kumar, V.; Sobti, A.; Toor, A.P. Enhanced photocatalytic activity of nickel and nitrogen codoped TiO₂ under sunlight. *Environ. Technol. Innov.* **2020**, *18*, 100658. [[CrossRef](#)]
18. Liu, X.; Li, Y.; Wei, Z.; Shi, L. A Fundamental DFT Study of Anatase (TiO₂) Doped with 3d Transition Metals for High Photocatalytic Activities. *J. Wuhan Univ. Technol. Mater. Sci. Ed.* **2018**, *33*, 403–408. [[CrossRef](#)]
19. Benjwal, P.; De, B.; Kar, K.K. 1-D and 2-D morphology of metal cation co-doped (Zn, Mn) TiO₂ and investigation of their photocatalytic activity. *Appl. Surf. Sci.* **2018**, *427*, 262–272. [[CrossRef](#)]
20. Shen, Q.; Wang, Y.; Xue, J.; Gao, G.; Liu, X.; Jia, H.; Li, Q.; Xu, B. The dual effects of RGO films in TiO₂/CdSe heterojunction: Enhancing photocatalytic activity and improving photocorrosion resistance. *Appl. Surf. Sci.* **2019**, *481*, 1515–1523. [[CrossRef](#)]
21. Kernazhitsky, L.; Shymanovska, V.; Gavrilko, T.; Naumov, V.; Kshnyakin, V.; Khalyavka, T. A comparative study of optical absorption and photocatalytic properties of nanocrystalline single-phase anatase and rutile TiO₂ doped with transition metal cations. *J. Solid State Chem.* **2013**, *198*, 511–519. [[CrossRef](#)]
22. Song, E.; Kim, Y.-T.; Choi, J. Anion additives in rapid breakdown anodization for nonmetal-doped TiO₂ nanotube powders. *Electrochem. Commun.* **2019**, *109*, 106610. [[CrossRef](#)]
23. Fadlallah, M.M. Magnetic, electronic, optical, and photocatalytic properties of nonmetal- and halogen-doped anatase TiO₂ nanotubes. *Phys. E Low Dimens. Syst. Nanostruct.* **2017**, *89*, 50–56. [[CrossRef](#)]
24. Varnagiris, S.; Medvids, A.; Lelis, M.; Milcius, D.; Antuzevics, A. Black carbon-doped TiO₂ films: Synthesis, characterization and photocatalysis. *J. Photochem. Photobiol. A Chem.* **2019**, *382*, 111941. [[CrossRef](#)]
25. Li, G.; Zou, B.; Feng, S.; Shi, H.; Liao, K.; Wang, Y.; Wang, W.; Zhang, G. Synthesis of N-Doped TiO₂ with good photocatalytic property. *Phys. B Condens. Matter* **2020**, *588*, 412184. [[CrossRef](#)]
26. Li, H.; Qiu, L.; Bharti, B.; Dai, F.; Zhu, M.; Ouyang, F.; Lin, L. Efficient photocatalytic degradation of acrylonitrile by Sulfur-Bismuth co-doped F-TiO₂/SiO₂ nanopowder. *Chemosphere* **2020**, *249*, 126135. [[CrossRef](#)]
27. He, D.; Li, Y.; Wu, J.; Yang, Y.; An, Q. Carbon wrapped and doped TiO₂ mesoporous nanostructure with efficient visible-light photocatalysis for NO removal. *Appl. Surf. Sci.* **2017**, *391*, 318–325. [[CrossRef](#)]
28. Boningari, T.; Inturi, S.N.R.; Suidan, M.; Smirniotis, P.G. Novel one-step synthesis of nitrogen-doped TiO₂ by flame aerosol technique for visible-light photocatalysis: Effect of synthesis parameters and secondary nitrogen (N) source. *Chem. Eng. J.* **2018**, *350*, 324–334. [[CrossRef](#)]
29. Jiang, J.X.; Zhang, Q.Q.; Li, Y.H.; Li, L. Three-dimensional network graphene aerogel for enhancing adsorption and visible light photocatalysis of nitrogen-doped TiO₂. *Mater. Lett.* **2019**, *234*, 298–301. [[CrossRef](#)]
30. Marques, J.; Gomes, T.D.; Forte, M.A.; Silva, R.F.; Tavares, C.J. A new route for the synthesis of highly-active N-doped TiO₂ nanoparticles for visible light photocatalysis using urea as nitrogen precursor. *Catal. Today* **2019**, *326*, 36–45. [[CrossRef](#)]
31. Du, M.; Qiu, B.; Zhu, Q.; Xing, M.; Zhang, J. Fluorine doped TiO₂/mesocellular foams with an efficient photocatalytic activity. *Catal. Today* **2019**, *327*, 340–346. [[CrossRef](#)]

32. Li, C.; Sun, Z.; Ma, R.; Xue, Y.; Zheng, S. Fluorine doped anatase TiO₂ with exposed reactive (001) facets supported on porous diatomite for enhanced visible-light photocatalytic activity. *Microporous Mesoporous Mater.* **2017**, *243*, 281–290. [[CrossRef](#)]
33. Wei, J.Q.; Chen, X.J.; Wang, P.F.; Han, Y.B.; Xu, J.C.; Hong, B.; Jin, H.X.; Jin, D.F.; Peng, X.L.; Li, J.; et al. High surface area TiO₂/SBA-15 nanocomposites: Synthesis, microstructure and adsorption-enhanced photocatalysis. *Chem. Phys.* **2018**, *510*, 47–53. [[CrossRef](#)]
34. Hafez, H.S. Synthesis of highly-active single-crystalline TiO₂ nanorods and its application in environmental photocatalysis. *Mater. Lett.* **2009**, *63*, 1471–1474. [[CrossRef](#)]
35. Vargas Hernández, J.; Coste, S.; García Murillo, A.; Carrillo Romo, F.; Kassiba, A. Effects of metal doping (Cu, Ag, Eu) on the electronic and optical behavior of nanostructured TiO₂. *J. Alloys Compd.* **2017**, *710*, 355–363. [[CrossRef](#)]
36. Belošević-Čavor, J.; Koteski, V.; Umićević, A.; Ivanovski, V. Effect of 5d transition metals doping on the photocatalytic properties of rutile TiO₂. *Comput. Mater. Sci.* **2018**, *151*, 328–337. [[CrossRef](#)]
37. Unal, F.A.; Ok, S.; Unal, M.; Topal, S.; Cellat, K.; Şen, F. Synthesis, characterization, and application of transition metals (Ni, Zr, and Fe) doped TiO₂ photoelectrodes for dye-sensitized solar cells. *J. Mol. Liq.* **2020**, *299*, 112177. [[CrossRef](#)]
38. Liu, L.; Zhang, X.; Yang, L.; Ren, L.; Wang, D.; Ye, J. Metal nanoparticles induced photocatalysis. *Natl. Sci. Rev.* **2017**, *4*, 761–780. [[CrossRef](#)]
39. Yao, G.Y.; Zhao, Z.Y.; Liu, Q.L.; Dong, X.D.; Zhao, Q.M. Theoretical calculations for localized surface plasmon resonance effects of Cu/TiO₂ nanosphere: Generation, modulation, and application in photocatalysis. *Sol. Energy Mater. Sol. Cells* **2020**, *208*, 110385. [[CrossRef](#)]
40. Kumaravel, V.; Mathew, S.; Bartlett, J.; Pillai, S.C. Photocatalytic hydrogen production using metal doped TiO₂: A review of recent advances. *Appl. Catal. B Environ.* **2019**, *244*, 1021–1064. [[CrossRef](#)]
41. Xiu, Z.; Guo, M.; Zhao, T.; Pan, K.; Xing, Z.; Li, Z.; Zhou, W. Recent advances in Ti³⁺ self-doped nanostructured TiO₂ visible light photocatalysts for environmental and energy applications. *Chem. Eng. J.* **2020**, *382*, 123011. [[CrossRef](#)]
42. Pulido Melián, E.; Nereida Suárez, M.; Jardiel, T.; Calatayud, D.G.; Del Campo, A.; Doña-Rodríguez, J.M.; Araña, J.; González Díaz, O.M. Highly photoactive TiO₂ microspheres for photocatalytic production of hydrogen. *Int. J. Hydrogen Energy* **2019**, *44*, 24653–24666. [[CrossRef](#)]
43. Huang, G.; Liu, X.; Shi, S.; Li, S.; Xiao, Z.; Zhen, W.; Liu, S.; Wong, P.K. Hydrogen producing water treatment through mesoporous TiO₂ nanofibers with oriented nanocrystals. *Chin. J. Catal.* **2020**, *41*, 50–61. [[CrossRef](#)]
44. Chen, W.; Wang, Y.; Liu, S.; Gao, L.; Mao, L.; Fan, Z.; Shangguan, W.; Jiang, Z. Non-noble metal Cu as a cocatalyst on TiO₂ nanorod for highly efficient photocatalytic hydrogen production. *Appl. Surf. Sci.* **2018**, *445*, 527–534. [[CrossRef](#)]
45. Gao, H.; Zhang, P.; Zhao, J.; Zhang, Y.; Hu, J.; Shao, G. Plasmon enhancement on photocatalytic hydrogen production over the Z-scheme photosynthetic heterojunction system. *Appl. Catal. B Environ.* **2017**, *210*, 297–305. [[CrossRef](#)]
46. El-Bery, H.M.; Matsushita, Y.; Abdel-moneim, A. Fabrication of efficient TiO₂-RGO heterojunction composites for hydrogen generation via water-splitting: Comparison between RGO, Au and Pt reduction sites. *Appl. Surf. Sci.* **2017**, *423*, 185–196. [[CrossRef](#)]
47. Wu, L.; Shi, S.; Li, Q.; Zhang, X.; Cui, X. TiO₂ nanoparticles modified with 2D MoSe₂ for enhanced photocatalytic activity on hydrogen evolution. *Int. J. Hydrogen Energy* **2019**, *44*, 720–728. [[CrossRef](#)]
48. Xing, X.; Zhu, H.; Zhang, M.; Xiao, L.; Li, Q.; Yang, J. Effect of heterojunctions and phase-junctions on visible-light photocatalytic hydrogen evolution in BCN-TiO₂ photocatalysts. *Chem. Phys. Lett.* **2019**, *727*, 11–18. [[CrossRef](#)]
49. Li, F.; Xiao, X.; Zhao, C.; Liu, J.; Li, Q.; Guo, C.; Tian, C.; Zhang, L.; Hu, J.; Jiang, B. TiO₂-on-C₃N₄ double-shell microtubes: In-situ fabricated heterostructures toward enhanced photocatalytic hydrogen evolution. *J. Colloid Interface Sci.* **2020**, *572*, 22–30. [[CrossRef](#)] [[PubMed](#)]
50. Zhang, C.; Zhou, Y.; Bao, J.; Fang, J.; Zhao, S.; Zhang, Y.; Sheng, X.; Chen, W. Structure regulation of ZnS@g-C₃N₄/TiO₂ nanospheres for efficient photocatalytic H₂ production under visible-light irradiation. *Chem. Eng. J.* **2018**, *346*, 226–237. [[CrossRef](#)]

51. Melián, E.P.; López, C.R.; Méndez, A.O.; Díaz, O.G.; Suárez, M.N.; Doña Rodríguez, J.M.; Navío, J.A.; Fernández Hevia, D. Hydrogen production using Pt-loaded TiO₂ photocatalysts. *Int. J. Hydrogen Energy* **2013**, *38*, 11737–11748. [[CrossRef](#)]
52. Vaiano, V.; Lara, M.A.; Iervolino, G.; Matarangolo, M.; Navio, J.A.; Hidalgo, M.C. Photocatalytic H₂ production from glycerol aqueous solutions over fluorinated Pt-TiO₂ with high {001} facet exposure. *J. Photochem. Photobiol. A Chem.* **2018**, *365*, 52–59. [[CrossRef](#)]
53. Yasuda, M.; Matsumoto, T.; Yamashita, T. Sacrificial hydrogen production over TiO₂-based photocatalysts: Polyols, carboxylic acids, and saccharides. *Renew. Sustain. Energy Rev.* **2018**, *81*, 1627–1635. [[CrossRef](#)]
54. López, C.R.; Melián, E.P.; Ortega Méndez, J.A.; Santiago, D.E.; Doña Rodríguez, J.M.; González Díaz, O. Comparative study of alcohols as sacrificial agents in H₂ production by heterogeneous photocatalysis using Pt/TiO₂ catalysts. *J. Photochem. Photobiol. A Chem.* **2015**, *312*, 45–54. [[CrossRef](#)]
55. Velázquez, J.J.; Fernández-González, R.; Díaz, L.; Pulido Melián, E.; Rodríguez, V.D.; Núñez, P. Effect of reaction temperature and sacrificial agent on the photocatalytic H₂-production of Pt-TiO₂. *J. Alloys Compd.* **2017**, *721*, 405–410. [[CrossRef](#)]
56. Kampouri, S.; Stylianou, K.C. Dual-Functional Photocatalysis for Simultaneous Hydrogen Production and Oxidation of Organic Substances. *ACS Catal.* **2019**, *9*, 4247–4270. [[CrossRef](#)]
57. Zhang, S.; Wang, L.; Liu, C.; Luo, J.; Crittenden, J.; Liu, X.; Cai, T.; Yuan, J.; Pei, Y.; Liu, Y. Photocatalytic wastewater purification with simultaneous hydrogen production using MoS₂ QD-decorated hierarchical assembly of ZnIn₂S₄ on reduced graphene oxide photocatalyst. *Water Res.* **2017**, *121*, 11–19. [[CrossRef](#)]
58. Bellardita, M.; García-López, E.I.; Marci, G.; Nasillo, G.; Palmisano, L. Photocatalytic Solar Light H₂ Production by Aqueous Glucose Reforming: Photocatalytic Solar Light H₂ Production by Aqueous Glucose Reforming. *Eur. J. Inorg. Chem.* **2018**, *2018*, 4522–4532. [[CrossRef](#)]
59. Yao, Y.; Gao, X.; Li, Z.; Meng, X. Photocatalytic Reforming for Hydrogen Evolution: A Review. *Catalysts* **2020**, *10*, 335. [[CrossRef](#)]
60. Park, Y.K.; Kim, B.J.; Jeong, S.; Jeon, K.J.; Chung, K.H.; Jung, S.C. Characteristics of hydrogen production by photocatalytic water splitting using liquid phase plasma over Ag-doped TiO₂ photocatalysts. *Environ. Res.* **2020**, *188*, 109630. [[CrossRef](#)]
61. Wu, G.; Chen, T.; Su, W.; Zhou, G.; Zong, X.; Lei, Z.; Li, C. H₂ production with ultra-low CO selectivity via photocatalytic reforming of methanol on Au/TiO₂ catalyst. *Int. J. Hydrogen Energy* **2008**, *33*, 1243–1251. [[CrossRef](#)]
62. Udayabhanu; Reddy, N.L.; Shankar, M.V.; Sharma, S.C.; Nagaraju, G. One-pot synthesis of Cu-TiO₂/CuO nanocomposite: Application to photocatalysis for enhanced H₂ production, dye degradation & detoxification of Cr (VI). *Int. J. Hydrogen Energy* **2020**, *45*, 7813–7828.
63. Xing, X.; Tang, S.; Hong, H.; Jin, H. Concentrated solar photocatalysis for hydrogen generation from water by titania-containing gold nanoparticles. *Int. J. Hydrogen Energy* **2020**, *45*, 9612–9623. [[CrossRef](#)]
64. Su, E.C.; Huang, B.S.; Lee, J.T.; Wey, M.Y. Excellent dispersion and charge separation of SrTiO₃-TiO₂ nanotube derived from a two-step hydrothermal process for facilitating hydrogen evolution under sunlight irradiation. *Sol. Energy* **2018**, *159*, 751–759. [[CrossRef](#)]
65. Sultanov, F.; Daulbayev, C.; Bakbolat, B.; Daulbayev, O.; Bigaj, M.; Mansurov, Z.; Kuterbekov, K.; Bekmyrza, K. Aligned composite SrTiO₃/PAN fibers as 1D photocatalyst obtained by electrospinning method. *Chem. Phys. Lett.* **2019**, *737*, 136821. [[CrossRef](#)]
66. Sultanov, F.; Bakbolat, B.; Mansurov, Z.; Pei, S.-S.; Ebrahim, R.; Daulbayev, C.; Urazgaliyeva, A.; Tulepov, M. Spongy Structures Coated with Carbon Nanomaterials for Efficient Oil/Water Separation. *Eurasian Chem. Technol. J.* **2017**, *19*, 127. [[CrossRef](#)]
67. Sultanov, F.; Bakbolat, B.; Daulbaev, C.; Urazgaliyeva, A.; Azizov, Z.; Mansurov, Z.; Tulepov, M.; Pei, S.S. Sorptive Activity and Hydrophobic Behavior of Aerogels Based on Reduced Graphene Oxide and Carbon Nanotubes. *J. Eng. Phys. Thermophys.* **2017**, *90*, 826–830. [[CrossRef](#)]
68. Luo, L.; Li, J.; Dai, J.; Xia, L.; Barrow, C.J.; Wang, H.; Jegatheesan, J.; Yang, M. Bisphenol A removal on TiO₂-MoS₂-reduced graphene oxide composite by adsorption and photocatalysis. *Process. Saf. Environ. Prot.* **2017**, *112*, 274–279. [[CrossRef](#)]
69. Nguyen, C.H.; Tran, M.L.; Tran, T.T.V.; Juang, R.S. Enhanced removal of various dyes from aqueous solutions by UV and simulated solar photocatalysis over TiO₂/ZnO/rGO composites. *Sep. Purif. Technol.* **2020**, *232*, 115962. [[CrossRef](#)]

70. Kumar, K.Y.; Saini, H.; Pandiarajan, D.; Prashanth, M.K.; Parashuram, L.; Raghu, M.S. Controllable synthesis of TiO₂ chemically bonded graphene for photocatalytic hydrogen evolution and dye degradation. *Catal. Today* **2020**, *340*, 170–177. [[CrossRef](#)]
71. Rajender, G.; Kumar, J.; Giri, P.K. Interfacial charge transfer in oxygen deficient TiO₂-graphene quantum dot hybrid and its influence on the enhanced visible light photocatalysis. *Appl. Catal. B Environ.* **2018**, *224*, 960–972. [[CrossRef](#)]
72. Ali, M.H.H.; Al-Afify, A.D.; Goher, M.E. Preparation and characterization of graphene—TiO₂ nanocomposite for enhanced photodegradation of Rhodamine-B dye. *Egypt. J. Aquat. Res.* **2018**, *44*, 263–270. [[CrossRef](#)]
73. Ton, N.N.T.; Dao, A.T.N.; Kato, K.; Ikenaga, T.; Trinh, D.X.; Taniike, T. One-pot synthesis of TiO₂/graphene nanocomposites for excellent visible light photocatalysis based on chemical exfoliation method. *Carbon* **2018**, *133*, 109–117. [[CrossRef](#)]
74. Lettieri, S.; Gargiulo, V.; Pallotti, D.K.; Vitiello, G.; Maddalena, P.; Alfè, M.; Marotta, R. Evidencing opposite charge-transfer processes at TiO₂/graphene-related materials interface through a combined EPR, photoluminescence and photocatalysis assessment. *Catal. Today* **2018**, *315*, 19–30. [[CrossRef](#)]
75. Shahbazi, R.; Payan, A.; Fattahi, M. Preparation, evaluations and operating conditions optimization of nano TiO₂ over graphene based materials as the photocatalyst for degradation of phenol. *J. Photochem. Photobiol. A Chem.* **2018**, *364*, 564–576. [[CrossRef](#)]
76. Khan, H.; Jiang, Z.; Berk, D. Molybdenum doped graphene/TiO₂ hybrid photocatalyst for UV/visible photocatalytic applications. *Sol. Energy* **2018**, *162*, 420–430. [[CrossRef](#)]
77. Sun, X.; Ji, S.; Wang, M.; Dou, J.; Yang, Z.; Qiu, H.; Kou, S.; Ji, Y.; Wang, H. Fabrication of porous TiO₂-RGO hybrid aerogel for high-efficiency, visible-light photodegradation of dyes. *J. Alloys Compd.* **2020**, *819*, 153033. [[CrossRef](#)]
78. Sultanov, F.R.; Mansurov, Z.A.; Daulbayev, C.; Urazgaliyeva, A.A.; Bakbolat, B.; Pei, S.-S. Study of Sorption Capacity and Surface Morphology of Carbon Nanomaterials/Chitosan Based Aerogels. *Eur. Chem. Technol. J.* **2016**, *18*, 19. [[CrossRef](#)]
79. Sultanov, F.R.; Pei, S.S.S.; Auyelkhanqyzy, M.; Smagulova, G.; Lesbayev, B.T.; Mansurov, Z.A. Aerogels Based on Graphene Oxide with Addition of Carbon Nanotubes: Synthesis and Properties. *Eur. Chem. Technol. J.* **2014**, *16*, 265–269. [[CrossRef](#)]
80. Ali, M.H.H.; Al-Qahtani, K.M.; El-Sayed, S.M. Enhancing photodegradation of 2,4,6 trichlorophenol and organic pollutants in industrial effluents using nanocomposite of TiO₂ doped with reduced graphene oxide. *Egypt. J. Aquat. Res.* **2019**, *45*, 321–328. [[CrossRef](#)]
81. Nadimi, M.; Ziarati Saravani, A.; Aroon, M.A.; Ebrahimian Pirbazari, A. Photodegradation of methylene blue by a ternary magnetic TiO₂/Fe₃O₄/graphene oxide nanocomposite under visible light. *Mater. Chem. Phys.* **2019**, *225*, 464–474. [[CrossRef](#)]
82. Park, K.; Ali, I.; Kim, J.O. Photodegradation of perfluorooctanoic acid by graphene oxide-deposited TiO₂ nanotube arrays in aqueous phase. *J. Environ. Manag.* **2018**, *218*, 333–339. [[CrossRef](#)] [[PubMed](#)]
83. Al Kausor, M.; Chakraborty, D. Facile fabrication of N-TiO₂/Ag₃PO₄@GO nanocomposite toward photodegradation of organic dye under visible light. *Inorg. Chem. Commun.* **2020**, *116*, 107907. [[CrossRef](#)]
84. Zhou, Q.; Wang, M.; Tong, Y.; Wang, H.; Zhou, X.; Sheng, X.; Sun, Y.; Chen, C. Improved photoelectrocatalytic degradation of tetrabromobisphenol A with silver and reduced graphene oxide-modified TiO₂ nanotube arrays under simulated sunlight. *Ecotoxicol. Environ. Saf.* **2019**, *182*, 109472. [[CrossRef](#)] [[PubMed](#)]
85. Zhao, Y.; Wang, G.; Li, L.; Dong, X.; Zhang, X. Enhanced activation of peroxymonosulfate by nitrogen-doped graphene/TiO₂ under photo-assistance for organic pollutants degradation: Insight into N doping mechanism. *Chemosphere* **2020**, *244*, 125526. [[CrossRef](#)]
86. Chen, F.; An, W.; Li, Y.; Liang, Y.; Cui, W. Fabricating 3D porous PANI/TiO₂-graphene hydrogel for the enhanced UV-light photocatalytic degradation of BPA. *Appl. Surf. Sci.* **2018**, *427*, 123–132. [[CrossRef](#)]
87. Ghasemi, A.; Azzouz, R.; Laipple, G.; Kabak, K.E.; Heavey, C. Optimizing capacity allocation in semiconductor manufacturing photolithography area—Case study: Robert Bosch. *J. Manuf. Syst.* **2020**, *54*, 123–137. [[CrossRef](#)]
88. Daulbaev, C.B.; Dmitriev, T.P.; Sultanov, F.R.; Mansurov, Z.A.; Aliev, E.T. Obtaining Three-Dimensional Nanosize Objects on a “3D Printer + Electrospinning” Machine. *J. Eng. Phys. Thermophys.* **2017**, *90*, 1115–1118. [[CrossRef](#)]

89. Liu, J.; Liu, H.; Zuo, X.; Wen, F.; Jiang, H.; Cao, H.; Pei, Y. Micro-patterned TiO₂ films for photocatalysis. *Mater. Lett.* **2019**, *254*, 448–451. [[CrossRef](#)]
90. Wang, Q.; Jin, R.; Zhang, M.; Gao, S. Solvothermal preparation of Fe-doped TiO₂ nanotube arrays for enhancement in visible light induced photoelectrochemical performance. *J. Alloys Compd.* **2017**, *690*, 139–144. [[CrossRef](#)]
91. Zhang, J.J.; Qi, P.; Li, J.; Zheng, X.C.; Liu, P.; Guan, X.X.; Zheng, G.P. Three-dimensional Fe₂O₃-TiO₂-graphene aerogel nanocomposites with enhanced adsorption and visible light-driven photocatalytic performance in the removal of RhB dyes. *J. Ind. Eng. Chem.* **2018**, *61*, 407–415. [[CrossRef](#)]
92. Lesbayev, A.B.; Smagulova, G.T.; Kim, S.; Prikhod'ko, N.G.; Manakov, S.M.; Guseinov, N.; Mansurov, Z.A. Solution-Combustion Synthesis and Characterization of Fe₃O₄ Nanoparticles. *Int. J. Self Propag. High Temp. Synth.* **2018**, *27*, 195–197. [[CrossRef](#)]
93. Soltani-nezhad, F.; Saljoqi, A.; Shamspur, T.; Mostafavi, A. Photocatalytic degradation of imidacloprid using GO/Fe₃O₄/TiO₂-NiO under visible radiation: Optimization by response level method. *Polyhedron* **2019**, *165*, 188–196. [[CrossRef](#)]
94. Rajoriya, S.; Bargole, S.; George, S.; Saharan, V.K.; Gogate, P.R.; Pandit, A.B. Synthesis and characterization of samarium and nitrogen doped TiO₂ photocatalysts for photo-degradation of 4-acetamidophenol in combination with hydrodynamic and acoustic cavitation. *Sep. Purif. Technol.* **2019**, *209*, 254–269. [[CrossRef](#)]
95. Isari, A.A.; Hayati, F.; Kakavandi, B.; Rostami, M.; Motevassel, M.; Dehghanifard, E. N, Cu co-doped TiO₂@functionalized SWCNT photocatalyst coupled with ultrasound and visible-light: An effective sono-photocatalysis process for pharmaceutical wastewaters treatment. *Chem. Eng. J.* **2020**, *392*, 123685. [[CrossRef](#)]
96. Wu, D.; Wang, X.; Wang, H.; Wang, F.; Wang, D.; Gao, Z.; Wang, X.; Xu, F.; Jiang, K. Ultrasonic-assisted synthesis of two dimensional BiOCl/MoS₂ with tunable band gap and fast charge separation for enhanced photocatalytic performance under visible light. *J. Colloid Interface Sci.* **2019**, *533*, 539–547. [[CrossRef](#)]
97. Ding, J.; Liu, Q.; Zhang, Z.; Liu, X.; Zhao, J.; Cheng, S.; Zong, B.; Dai, W.L. Carbon nitride nanosheets decorated with WO₃ nanorods: Ultrasonic-assisted facile synthesis and catalytic application in the green manufacture of dialdehydes. *Appl. Catal. B Environ.* **2015**, *165*, 511–518. [[CrossRef](#)]



© 2020 by the authors. Licensee MDPI, Basel, Switzerland. This article is an open access article distributed under the terms and conditions of the Creative Commons Attribution (CC BY) license (<http://creativecommons.org/licenses/by/4.0/>).